

EQUILIBRIUM THERMODYNAMICS OF LATTICE QCD

D. K. Sinclair

*HEP Division, Argonne National Laboratory, 9700 South Cass Avenue, Argonne, IL,
60439, USA*

Lattice QCD allows us to simulate QCD at non-zero temperature and/or densities. Such equilibrium thermodynamics calculations are relevant to the physics of relativistic heavy-ion collisions. I give a brief review of the field with emphasis on our work.

1. Introduction

High temperature hadronic matter was certainly present in the early universe. Relativistic heavy-ion colliders such as RHIC and in future the LHC with heavy-ions, produce hot hadronic matter. Lower energy machines can produce hot hadronic matter with an appreciable baryon/quark-number density – hot nuclear matter. At high enough temperatures this hadronic matter is expected to become quark/gluon matter – the quark-gluon plasma. Preliminary evidence for the quark-gluon plasma has been reported from RHIC and CERN.

At high baryon/quark-number density and low temperature such as might exist in the cores of neutron stars, exotic states of matter, such as colour superconducting phases have been proposed.

In Quantum Chromodynamics (QCD), the accepted theory of hadrons and their strong interactions, the most interesting finite-temperature properties are non-perturbative. Lattice QCD simulations are the only systematic approach to the study of such phenomena.

Fig. 1 shows a simplified version of the proposed phase diagram. (For an introduction to the phase structure of QCD and predictions from lattice QCD, see recent reviews^{1,2}).

In Lattice QCD, we only really know how to calculate equilibrium thermodynamics. Relativistic heavy-ion collisions are clearly not equilibrium processes, but knowledge of equilibrium thermodynamics and the consequent extraction of thermodynamic quantities and the prediction of the

QCD at finite baryon density

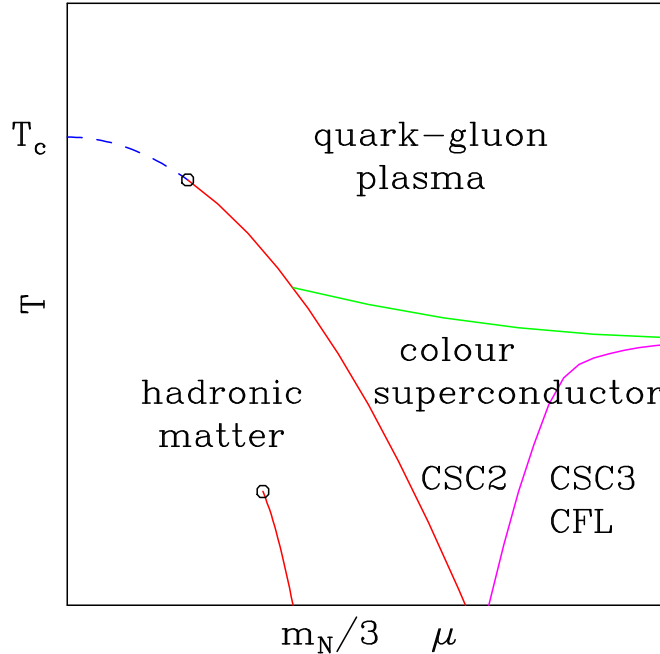


Fig. 1. Simplified phase diagram for QCD at finite temperature and quark-number chemical potential μ .

equation-of-state give us some idea of the type of behaviour we might expect. In addition, it can provide input for hydrodynamic models of such collisions.

QCD at finite temperature and/or densities yields information on the dynamics of confinement and chiral symmetry breaking and thus enhances our understanding of QCD.

2. Lattice QCD at finite temperature

QCD is quantized by functional integral methods. To make these integrals well-defined, we rotate to imaginary time – Euclidean space-time. The quark fields are then defined on the sites of a 4-dimensional hypercubic lattice, the gauge fields $U_\mu = \exp(igA_\mu)$ on its links.

$$Z = \int \mathcal{D}\psi \mathcal{D}\bar{\psi} \mathcal{D}U e^{-S} \quad (1)$$

where the action $S = S_f + S_g$. The simplest lattice implementation (which preserves gauge invariance) has

$$S_g = \beta \sum_{\square} \left(1 - \frac{1}{3} \text{ReTr}_{\square} UUUU \right), \quad (2)$$

where $\beta = 6/g^2$, and $S_f = \sum_{\text{sites}} \bar{\psi}(\not{D} + m)\psi$.

Simulations are performed by replacing the fermion fields with boson fields (pseudo-fermions) which results in replacing the Dirac operator by its inverse. Adding a ‘kinetic’ term for the gauge fields, allowing them to evolve in a fictitious ‘time’, turns Z into the partition function for a system of classical particles. One then uses molecular-dynamics techniques to effectively ‘evaluate’ the integrals, by numerically integrating the equations of motion for this system. Bringing the system in contact with a heat-bath at regular intervals assures ergodicity and compensates for the lack of dynamics for the pseudo-fermion fields.

To compensate for the doubling problems for the fermion fields frequently requires taking fractional powers of the fermion determinant. This is performed by using rational approximations to fractional powers of the Dirac operator. Use of a global Metropolis accept/reject step removes the discretization errors in the numerical integration of the equations of motion. (For a recent description of simulation methods with dynamical fermions see³).

If we use a lattice of temporal extent $1/T$ and a spatial extent much larger than this, and demand periodic boundary conditions for the gauge fields and antiperiodic boundary conditions for the fermion fields in the time direction, $Z = Z(T)$ the partition function for lattice QCD at temperature T .

3. The finite temperature transition

For massless quarks, chiral symmetry is restored at the finite temperature transition. $\langle \bar{\psi}\psi \rangle \neq 0$ below the transition and $\langle \bar{\psi}\psi \rangle = 0$ above the transition. Hence this transition is a phase transition. Arguments based on dimensional reduction predict that this phase transition is a second order phase transition (critical point) for $N_f = 2$, in the universality class of the 3-dimensional $O(4)$ spin model.⁴ For non-zero quark mass it is expected to weaken to a crossover with no real phase transition. For $N_f > 2$ this transition is predicted to be a first-order phase transition which is expected to remain first-order for small quark masses, becoming a crossover for larger quark masses.

In the real world where $N_f = 2 + 1$ (u, d, s), the important question is whether the strange quark mass is light enough for the transition to be first-order or whether it is a crossover. Recent lattice simulations indicate that the strange quark mass is too large, and the transition is a crossover⁵ (see Fig 2). This extends earlier work of⁸ (NB the $N_f = 3$ point agrees with

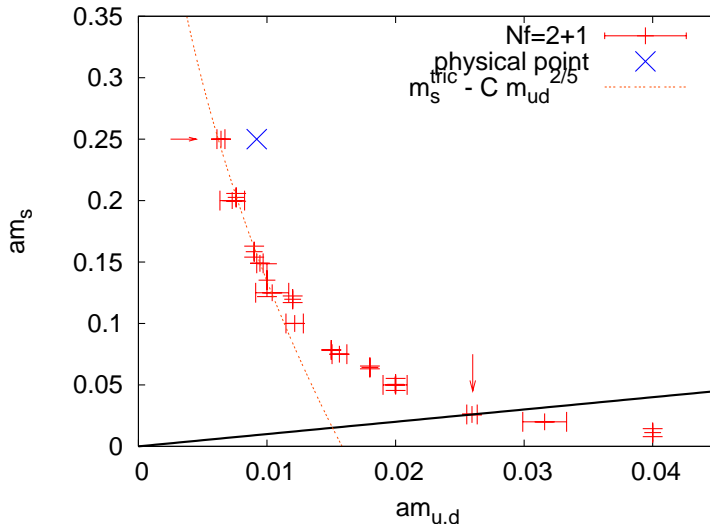


Fig. 2. The chiral critical line at zero baryon-number density (from Ref.⁵).

our own simulations.)

Simulations with larger lattices, finer lattice spacings and improved actions have recently been reported by.⁶ Here the u , d and s quark masses are chosen by fixing m_K/m_π (and f_K/f_π) at their physical values. Making several choices of masses restricted in this manner, they were able to extrapolate to the physical quark masses and below. They confirm the observation that the physical transition is a crossover and not a phase transition, in simulations which probe much closer to the continuum limit than in.⁵ The same simulations give new estimates for the temperature(s) of this crossover.⁷

Since the strange quark appears too massive to control the nature of the transition, it is useful to study the 2-flavour case, to see if the nature of the $m = 0$ phase transition agrees with the above prediction.

Determining the nature of the 2-flavour phase transition has proved difficult, since it is expected only at $m = 0$, and finite volume effects appear

to be large.^{9–12} Standard (including highly improved) lattice actions forbid simulations at $m = 0$, and small mass simulations are very expensive. No such simulations have been performed at masses small enough to uncover the $m = 0$ results.

We have performed $N_f = 2$ simulations using the χ QCD action which allows simulations at zero quark mass.¹³ Since it is a staggered quark action, the reduced flavour symmetry leads us to predict that the phase transition should be second-order and in the universality class of the 3-dimensional $O(2)$ spin model. To accommodate the finite volume effects, we compare our chiral condensate measurements to the magnetization of the $O(2)$ spin model also on finite volumes, as shown in Fig. 3. The agreement is excellent. Good agreement is also obtained with correlation lengths and susceptibilities.

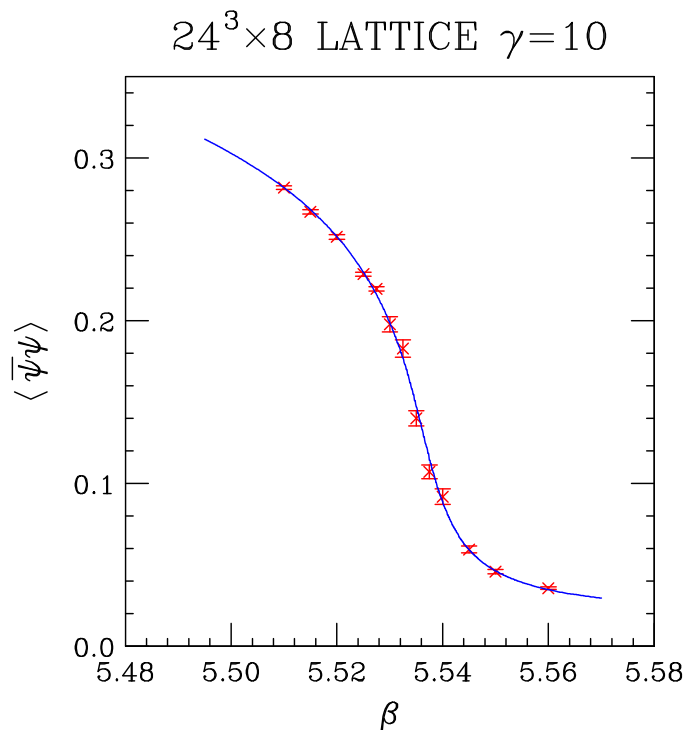


Fig. 3. Chiral condensate (points) near the chiral phase transition for lattice QCD, fitted to the magnetization (solid line) for the $O(2)$ spin model (from Ref.¹³).

Fig. 4 shows recent estimates of the transition temperature T_c from lattice QCD simulations, compared with an experimental estimate from RHIC. All lattice simulations are consistent with the chiral and deconfinement transitions being coincident.

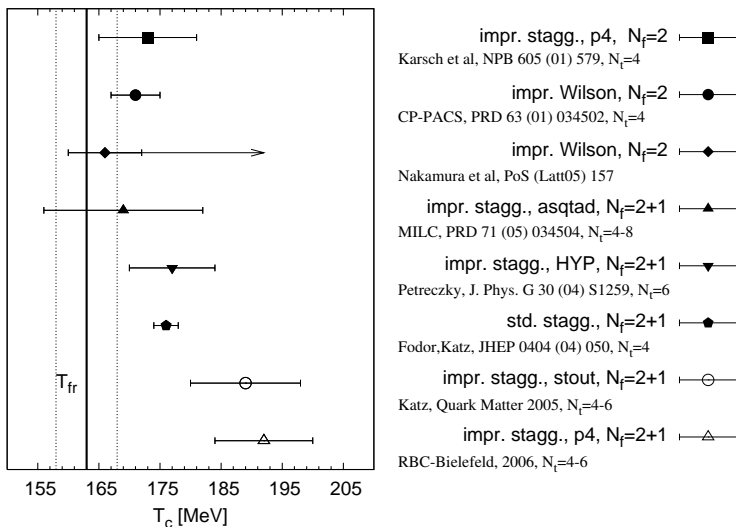


Fig. 4. Recent lattice estimates of T_c compared with experiment (from Ref.¹⁴).

4. The equation-of-state for hot QCD.

The equation-of-state (EOS) expresses the pressure p , the entropy density s and the energy density ϵ as functions of the temperature T . The free energy density, pressure and entropy are given by

$$f = -\frac{T}{V} \ln Z(T), \quad p = -f, \quad s = \frac{dp}{dT}, \quad (3)$$

respectively. The energy density is not an independent quantity but is given by

$$\epsilon = Ts - p. \quad (4)$$

$Z(T)$ is calculated on the lattice by numerically integrating

$$\frac{d \ln Z}{d\beta} = \langle S_g \rangle. \quad (5)$$

To obtain T as a function of β requires knowing the lattice spacing as a function of β . This can be obtained by measuring physical quantities as functions of β at zero temperature.

Knowledge of the EOS is needed as input to models for the evolution of the hot hadronic matter in relativistic heavy-ion collisions. Fig. 5 is a graph of these quantities from the MILC collaboration.¹⁵

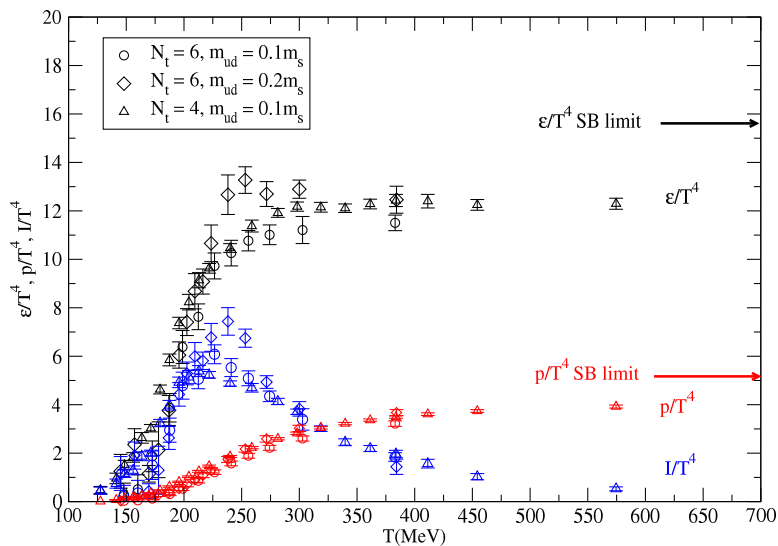


Fig. 5. The EOS from Lattice QCD simulations (MILC preliminary: status Lattice2006¹⁶). $I = \epsilon - 3p$

For earlier work on the finite temperature EOS see for example.¹⁷ Karsch *et al.* have shown that the low temperature behaviour is well modeled as a non-interacting gas of hadron resonances.¹⁸ See also¹⁹ for other work on the QCD EOS.

5. Meson spectral functions at finite T

Meson spectral functions yield information about the propagation of mesons, or excitations with mesonic quantum numbers in hot hadronic matter²⁰ (This review gives references to earlier works). Even just above T_c , the quark-gluon plasma is a strongly interacting fluid and mesonic states survive. Not only do the spectral functions have information about hadronic stability at high temperatures, but they also have information about transport coefficients and dilepton production. At zero temperature, the spectral

function is just the momentum space propagator. The Euclidean-time meson propagator $G(\tau, \mathbf{p}, T)$ is related to the spectral function $\sigma(\omega, \mathbf{p}, T)$ by

$$G(\tau, \mathbf{p}, T) = \int_0^\infty d\omega \sigma(\omega, \mathbf{p}, T) K(\tau, \omega, T) \quad (6)$$

where $K(\tau, \omega, T) = \frac{\cosh[\omega(\tau-1/2T)]}{\sinh(\omega/2T)}$.

The main difficulty has been that, since the spatial extent of the lattice must be much greater than its temporal extent, the temporal extent of the lattice is typically ~ 10 or less in lattice units. This gives a rather poor estimate of σ . Recently simulations have been performed on anisotropic lattices on which the spatial lattice spacing is much greater than the temporal lattice spacing.^{21,22} This allows for many more points in the time direction, while still keeping the spatial extent of the lattice much greater than its temporal extent. This leads to better estimates for the spectral functions.

The charmonium spectral functions have been of particular interest. It had been suggested that one signal for the quark-gluon plasma phase could be the ‘melting’ of charmonium. This would reveal itself as a drop in the charmonium production relative to the production of $D\bar{D}$ pairs and similar states.

Current simulations by the TrinLat collaboration using anisotropic lattices with dynamical light quarks, indicate that the J/ψ and η_c survive above T_c and melt somewhere between $1.3T_c$ and $2T_c$. The χ_c states appear to melt at or below $1.3T_c$ (see Fig. 6).

At the LHC, even higher temperatures are expected, and it has been suggested that these might be high enough to melt bottomonia.²³ We plan to measure NRQCD bottomonium propagators (and hence spectral functions) on the TrinLat configurations to determine these melting temperatures.

6. Transport coefficients

To use hydrodynamic models for hadronic matter in relativistic heavy-ion collisions requires knowledge of the transport coefficients, shear viscosity η , volume viscosity ζ and thermal conductivity κ . These viscosities are expressed in terms of Green’s functions of the stress-energy tensor.^{24,25}

$$\begin{aligned} \eta &= - \int d^3x' \int_{-\infty}^t dt_1 e^{\epsilon(t_1-t)} \int_{-\infty}^{t_1} dt' \langle T_{12}(\mathbf{x}, t) T_{12}(\mathbf{x}', t') \rangle_{ret} \\ \frac{4}{3}\eta + \zeta &= - \int d^3x' \int_{-\infty}^t dt_1 e^{\epsilon(t_1-t)} \int_{-\infty}^{t_1} dt' \langle T_{11}(\mathbf{x}, t) T_{11}(\mathbf{x}', t') \rangle_{ret} \end{aligned} \quad (7)$$

These real-time Green’s functions are obtained from their lattice (Euclidean time) counterparts through the spectral function $\sigma(\omega)$. Quenched

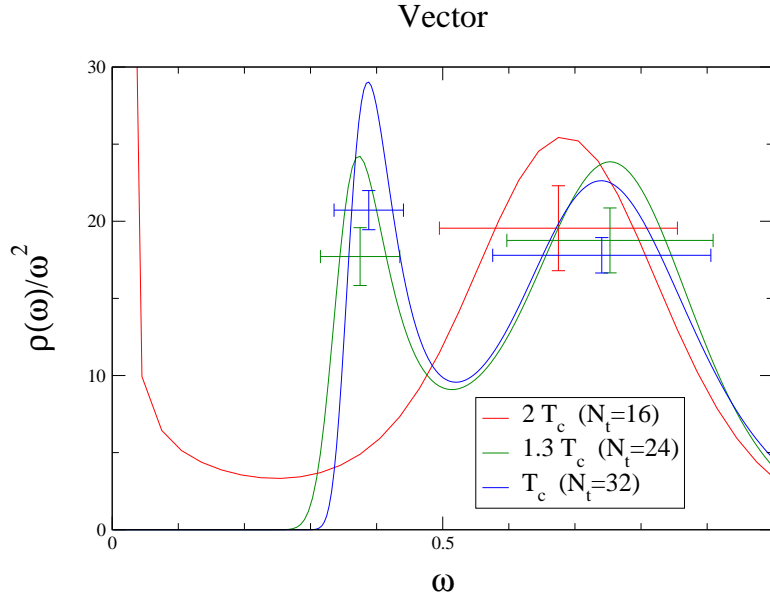


Fig. 6. Spectral function $\rho \equiv \sigma$ for the J/ψ at T_c , $1.3T_c$ and $2T_c$ (from Ref.²²).

lattice results have been obtained for these quantities.²⁶ In terms of the spectral function, $\eta = \pi \lim_{\omega \rightarrow 0} \frac{\sigma(\omega)}{\omega}$.

This means that one needs the spectral function near $\omega = 0$, where it is least well known. Thus the determination is difficult, and systematic as well as statistical errors are large as shown in Fig. 7. The same paper finds $\zeta \approx 0$. Clearly there is a long way to go.

More recently, improved methods have been used to calculate the electrical conductivity of the quark-gluon plasma.²⁷

7. Lattice QCD at finite baryon number density

Finite baryon/quark-number density is implemented by introduction of a quark-number chemical potential μ . On the lattice this is achieved by multiplying each of the links in the $+t$ direction by e^μ and each of those in the $-t$ direction by $e^{-\mu}$ in the quark action S_f .

Integrating out the fermion fields gives the determinant of the Dirac operator which is complex, with a real part of indefinite sign. Standard simulation methods, which rely on importance sampling, fail for such systems.

Some progress has been made in circumventing these problems for small

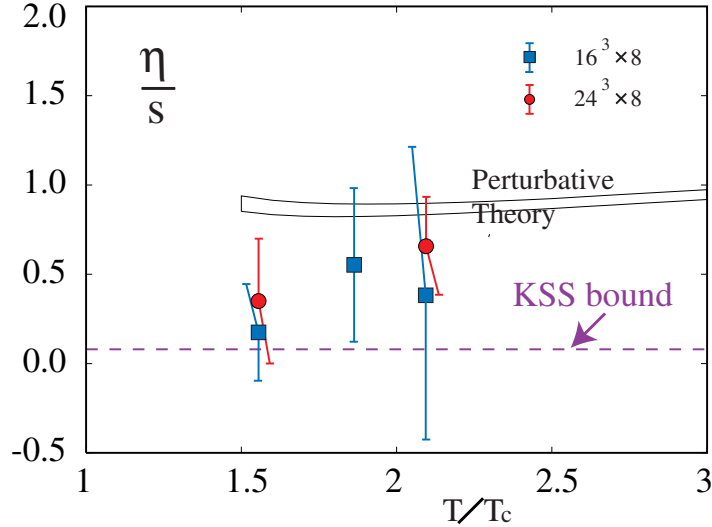


Fig. 7. η/s as a function of temperature. Dashed line is at $1/4\pi$ (from Ref.²⁶).

μs close to the finite temperature transition. Methods for doing this fall into several classes.

- Analytic continuation: In the simplest case people simulate at imaginary μs , where the fermion determinant is real and positive. The results are fitted to a power series in μ^2 , which allows continuation to real μ .^{28,29} Fancier analytic continuation methods have also been used.³⁰
- Power series expansions: These are similar in spirit to the analytic continuation methods. The exponential of the action is expanded in powers of μ^2 . The coefficients of this expansion are then observables whose expectation values are measured in $\mu = 0$ simulations.^{31,32}
- Reweighting methods: These start from a quark action with a positive fermion determinant, and reweight measurements by the ratio of the original fermion determinant to this positive fermion determinant. One then divides by the expectation value of this ratio of determinants.³³
- Phase quenched methods: One simulates using the magnitude of the fermion determinant ignoring the phase. For small enough μ on a finite lattice, the phase is small enough that this should yield

the same phase structure as the full simulation.³⁴

- Canonical ensemble methods: The fermion determinant is projected on to states of fixed quark number. One deals with any sign problems by reweighting.³⁵

For 3-flavour QCD, it has been argued that the critical point observed at zero chemical potentials, where the transition weakens from a first-order phase transition to a crossover, would move to larger quark masses as μ is increased from zero, becoming the sort-after critical endpoint. Recent work using analytic continuation from imaginary μ (de Forcrand and Philipsen²⁸) and simulations in the phase-quenched theory (Kogut and Sinclair),³⁴ indicate that this does not happen. Instead, the critical mass appears to decrease with increasing μ .

Fodor and Katz, using the reweighting method, claim to find the critical endpoint, for physical quark masses.³³ Their estimate of its position is $T = 162(2)$ MeV and $\mu = 120(13)$ MeV. Since $\mu > m_\pi/2$, this is beyond the reach of analytic continuation, phase quenched and series expansion methods. It remains to develop other methods which could check this. Fig. 8

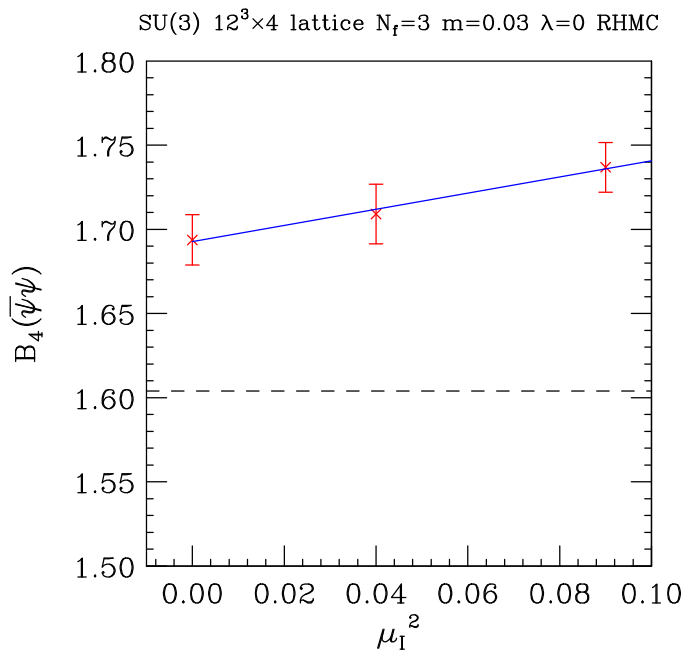


Fig. 8. Binder cumulant for the chiral condensate as a function of μ_I (from Ref.³⁴).

shows the behaviour of the Binder cumulant in the phase-quenched theory. If there were a critical endpoint at (small) finite μ_I , this Binder cumulant would decrease through the Ising value 1.604(1) (dashed line). Instead it increases indicating that there is no critical endpoint in this range of μ_I .

8. The EOS at non-zero T and μ

At finite temperature and small μ , the series expansions in terms of μ also enable one to calculate such quantities as p , s and ϵ and hence to study the equation-of-state in terms of T and μ .³⁶ Similar results have been obtained using multi-parameter reweighting techniques.³⁷

The pressure p can be obtained from measurement of the quark-number density ρ , since

$$\rho = \frac{\partial p}{\partial \mu}. \quad (8)$$

The pressure at zero μ is calculated as above. That at finite μ can be obtained by integrating the previous equation. ϵ can also be calculated, but requires knowledge of the running of the coupling constant and quark mass. Results from the Bielefeld group are shown in Fig. 9

9. Summary and Conclusions

Lattice QCD at finite temperature can probe the nature of the phase transition from hadronic matter to a quark-gluon plasma. For physical quark masses this appears to be a crossover without a true phase transition, influenced by the second-order transition at $m_u = m_d = 0$.

The QCD equation-of-state and other equilibrium thermodynamic quantities measured in lattice QCD simulations provide input for an understanding of the non-equilibrium thermodynamics at RHIC and the LHC. Finite temperature (lattice) QCD probes QCD dynamics such as confinement and chiral-symmetry breaking.

Charmonium spectral functions show that the J/ψ remains intact at the finite temperature transition T_c , but dissociates below $2T_c$. This should produce a reduction in J/ψ 's from the most energetic processes at RHIC. Bottomonium spectral functions should show similar behaviour at the even higher temperatures of the LHC heavy-ion program.

Just above T_c , the 'deconfined' phase is a strongly-interacting fluid with low viscosity. Transport coefficients (including viscosity) need to be calculated as input for hydrodynamic models. Early attempts have been made in lattice QCD simulations, but such measurements are difficult.

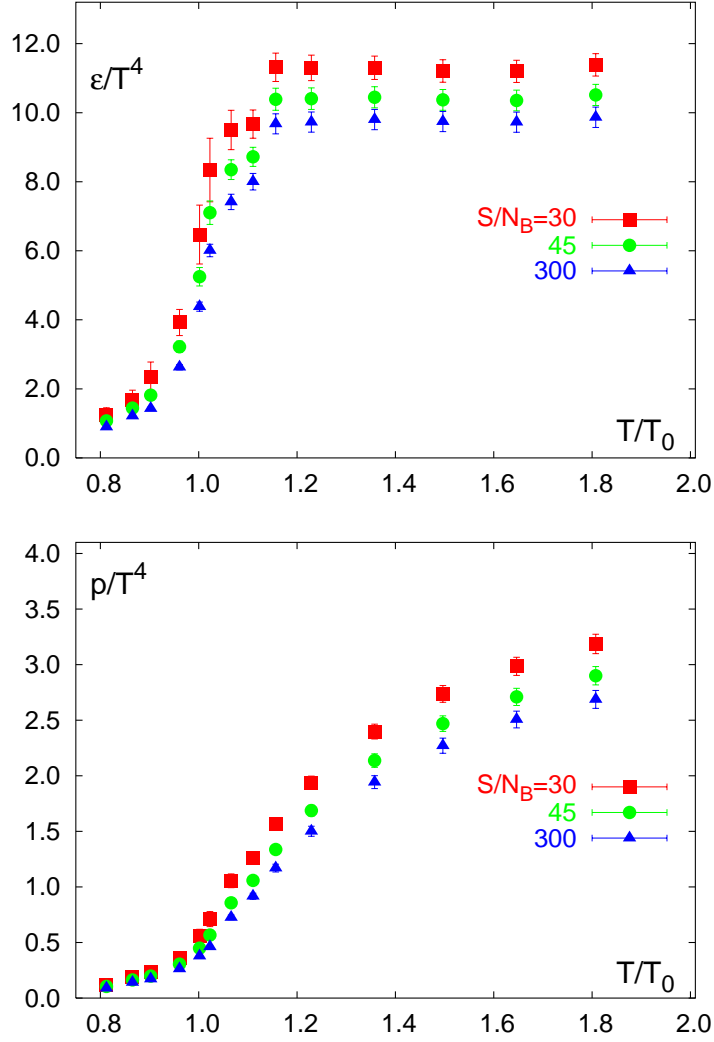


Fig. 9. ϵ and p as functions of T (from Ref.³⁶).

Sign problems hamper simulations at finite baryon/quark-number density. Some progress has been made for small μ_s close to the finite temperature transition. The equation-of-state has been determined in this high-temperature low baryon-number-density regime. More work is needed to observe the critical endpoint, which is the most striking feature expected

in this region of the QCD phase diagram. This is a region accessible experimentally to lower-energy relativistic heavy-ion collisions.

New methods will be needed if one is ever to reach the high baryon-number densities needed to understand the physics of neutron stars. At such densities one expects such exotic states of matter as colour superconductors.

Acknowledgements

Research supported by U.S. Department of Energy contract DE-AC-02-06CH11357. I thank the authors of the manuscripts, from which some of the figures were reproduced, for their permission to incorporate these figures in this manuscript. My own research reported in this talk was performed in collaboration with J. B. Kogut.

References

1. U. M. Heller, PoS **LAT2006**, 011 (2006) [arXiv:hep-lat/0610114].
2. M. G. Alford, Ann. Rev. Nucl. Part. Sci. **51**, 131 (2001) [arXiv:hep-ph/0102047].
3. A. D. Kennedy, arXiv:hep-lat/0607038.
4. R. D. Pisarski and F. Wilczek, Phys. Rev. D **29**, 338 (1984).
5. P. de Forcrand and O. Philipsen, arXiv:hep-lat/0607017.
6. Y. Aoki, G. Endrodi, Z. Fodor, S. D. Katz and K. K. Szabo, Nature **443**, 675 (2006) [arXiv:hep-lat/0611014].
7. Y. Aoki, Z. Fodor, S. D. Katz and K. K. Szabo, Phys. Lett. B **643**, 46 (2006) [arXiv:hep-lat/0609068].
8. F. Karsch, E. Laermann and C. Schmidt, Phys. Lett. B **520**, 41 (2001) [arXiv:hep-lat/0107020].
9. F. Karsch, Phys. Rev. D **49**, 3791 (1994) [arXiv:hep-lat/9309022].
10. F. Karsch and E. Laermann, Phys. Rev. D **50**, 6954 (1994) [arXiv:hep-lat/9406008].
11. S. Aoki *et al.* [JLQCD Collaboration], Phys. Rev. D **57**, 3910 (1998) [arXiv:hep-lat/9710048].
12. C. W. Bernard *et al.* [MILC Collaboration], Phys. Rev. D **55**, 6861 (1997) [arXiv:hep-lat/9612025].
13. J. B. Kogut and D. K. Sinclair, Phys. Rev. D **73**, 074512 (2006) [arXiv:hep-lat/0603021].
14. P. Petreczky, arXiv:hep-lat/0609040.
15. C. Bernard *et al.*, arXiv:hep-lat/0611031.
16. C. Bernard *et al.*, arXiv:hep-lat/0610017.
17. F. Karsch, E. Laermann and A. Peikert, Phys. Lett. B **478**, 447 (2000) [arXiv:hep-lat/0002003].
18. F. Karsch, K. Redlich and A. Tawfik, Eur. Phys. J. C **29**, 549 (2003) [arXiv:hep-ph/0303108].

19. Y. Aoki, Z. Fodor, S. D. Katz and K. K. Szabo, *JHEP* **0601**, 089 (2006) [arXiv:hep-lat/0510084].
20. P. Petreczky, *Nucl. Phys. Proc. Suppl.* **140**, 78 (2005) [arXiv:hep-lat/0409139].
21. A. Jakovac, P. Petreczky, K. Petrov and A. Velytsky, arXiv:hep-lat/0611017.
22. G. Aarts, C. R. Allton, R. Morrin, A. P. O. Cais, M. B. Oktay, M. J. Peardon and J. I. Skullerud, arXiv:hep-lat/0610065.
23. J. F. Gunion and R. Vogt, *Nucl. Phys. B* **492**, 301 (1997) [arXiv:hep-ph/9610420].
24. R. Horsley and W. Schoenmaker, *Nucl. Phys. B* **280**, 716 (1987).
25. R. Horsley and W. Schoenmaker, *Nucl. Phys. B* **280**, 735 (1987).
26. A. Nakamura and S. Sakai, *Phys. Rev. Lett.* **94**, 072305 (2005) [arXiv:hep-lat/0406009].
27. S. Gupta, *Phys. Lett. B* **597**, 57 (2004) [arXiv:hep-lat/0301006].
28. P. de Forcrand and O. Philipsen, arXiv:hep-lat/0611027.
29. M. D'Elia and M. P. Lombardo, *Phys. Rev. D* **70**, 074509 (2004) [arXiv:hep-lat/0406012].
30. V. Azcoiti, G. Di Carlo, A. Galante and V. Laliena, *Nucl. Phys. B* **723**, 77 (2005) [arXiv:hep-lat/0503010].
31. S. Ejiri, C. R. Allton, S. J. Hands, O. Kaczmarek, F. Karsch, E. Laermann and C. Schmidt, *Prog. Theor. Phys. Suppl.* **153**, 118 (2004) [arXiv:hep-lat/0312006].
32. R. V. Gavai and S. Gupta, *Phys. Rev. D* **71**, 114014 (2005) [arXiv:hep-lat/0412035].
33. Z. Fodor and S. D. Katz, *JHEP* **0404**, 050 (2004) [arXiv:hep-lat/0402006].
34. D. K. Sinclair and J. B. Kogut, arXiv:hep-lat/0609041.
35. S. Kratochvila and P. de Forcrand, *PoS LAT2005*, 167 (2006) [arXiv:hep-lat/0509143].
36. S. Ejiri, F. Karsch, E. Laermann and C. Schmidt, *Phys. Rev. D* **73**, 054506 (2006) [arXiv:hep-lat/0512040].
37. F. Csikor, G. I. Egri, Z. Fodor, S. D. Katz, K. K. Szabo and A. I. Toth, *JHEP* **0405**, 046 (2004) [arXiv:hep-lat/0401016].